Model-Based Prediction of Amplitude Scintillation Variance Due to Clear-Air Tropospheric Turbulence on Earth-Satellite Microwave Links

Frank S. Marzano and Giovanni d'Auria

***Abstract*— A statistical method to predict tropospheric amplitude scintillation parameters along earth-space microwave links from meteorological data is proposed. The evaluation of the mean value and the variance of the refractive-index structure constant and of the scintillation power (i.e., the variance of the log-amplitude fluctuations of the received electromagnetic field) is carried out from conventional radio-sounding measurements. A large radio-sounding data set, collected in Northern Italy over ten years is utilized to simulate clear-air amplitude scintillation variance at microwaves and millimeter-waves on slant paths. Scintillation statistics of interest for link-budget design are also derived from the radio-sounding data set for short and long-term applications. Scintillation prediction formulas, based on measurements of surface temperature and relative humidity, are also derived and regression coefficient tables are given on an hourly and a monthly basis. Comparisons of short-term and long-term prediction results with Olympus down-link measurements at 19.8 GHz are shown and discussed. A model investigation about the statistical correlation between scintillation power and brightness temperature is performed, deriving an extension of the estimation methods to include integrated water vapor measurements from ground-based microwave radiometers.**

***Index Terms*— Meteorology, microwave propagation, random media, satellite communication.**

I. Introduction

ONE of the major problems in the link budget design of microwave and millimeter-wave communication systems is represented by tropospheric scintillation, i.e., rapid fluctuations of the signal amplitude and phase due to tropospheric turbulence [1]. Scintillation phenomena can cause a significant degradation of the signal-to-noise ratio (up to several decibels) and their effects increase with the increase of channel frequency and the decrease of the antenna aperture and elevation angle [2], [3]. The analysis of the tropospheric scintillation impact is gaining a renewed interest due to the introduction of mobile and fixed digital telecommunications in the K-band based on very small aperture terminals (VSAT), clusters of low-elevation orbit (LEO) satellites and wireless multipoint distribution services (MDS) with link margins for high availability [4]–[6]. In these cases, scintillation effects become a relevant noise source, which has to be considered and predicted for the optimum utilization of the channel capacity [7].

Satellite propagation experiments have pioneered the exploitation of new frequency bands for commercial and scientific applications. In the last few years, first the Olympus experiment and then the Italsat program (still operating) have been some of the most important international experiments carried out in the 10–50 GHz bands [8]. However, since these experiments are not always easy to set up and are generally expensive within the link design budget, there is also an interest in developing methods for predicting tropospheric amplitude scintillation directly from meteorological data. These statistical relationships can be derived, on one hand, by collecting experimental data of meteorological variables corresponding to received scintillation power [9]–[12]. On the other hand, it is possible to resort to a modeling approach; that is, to use an interaction model between microwave radiation and turbulent medium to evaluate the received scintillation power and its spectrum in a given frequency band and for a given elevation angle [13], [14].

One of the main advantages in adopting the modeling approach is the capability to derive the scintillation statistics without needing satellite measurements for the considered site. However, in this case the prediction methods strongly rely on the accuracy of the interaction model used. The common assumption is to assume the atmosphere to be horizontally stratified and characterized by vertical profiles of meteorological measurements acquired at given levels by radio-sounding balloons [9], [14]. The simulation approach can be also used to determine statistical prediction methods of scintillation variance from surface meteorological data [6]. This possibility is very appealing since in most ground-stations surface meteorological sensors are installed and, in any case, surface data are very easy (and economical) to acquire with respect to radio soundings.

In the last years many satellite receiving stations have been also equipped with multichannel microwave radiometers, generally pointed along the link slant path [15]. The main purpose of using microwave radiometers is to estimate the total path attenuation together with the vertically integrated water vapor content and cloud liquid water content [16], [17]. A correlation between scintillation and brightness temperature measurements has been already illustrated in literature by using experimental data [3], [18]. This correlation can be also investigated by using radiative transfer and scintillation models

Manuscript received October 7, 1997; revised June 5, 1998.

F. S. Marzano is with the Dipartimento di Ingegneria Elettrica, Università dell'Aquila, Monteluco di Roio, 67040 L'Aquila, Italy.

G. d'Auria is with the Dipartimento di Ingegneria Elettronica, Università "La Sapienza" di Roma, Via Eudossiana, 18-00184 Roma, Italy.

Publisher Item Identifier S 0018-926X(98)07499-7.

in order to introduce the atmospheric parameters estimated by microwave radiometers within model-based scintillation prediction methods.

In this work, a model of C_n^2, which takes into account the turbulence intermittence as a random process, is applied. The formulation of the random model of C_n^2 basically involves both the Richardson number to describe the local atmospheric instability and the Tatarskii theory of homogeneous turbulence. In Section II, the calculation of the mean value and variance of C_n^2 is carried out by expressing the mean value of C_n^2 in intermittent turbulence through mean values of meteorological variables and gradients, directly derivable from conventional radio-sounding observations (RAOB's). In Section III, a ten-year RAOB data set is used in order to simulate the statistical distribution of the structure constant and of the received scintillation power for a microwave slant link at 19.8 GHz and elevation angle of 30.6°. In Section IV, scintillation prediction formulas from surface meteorological data are developed using the multivariate regression analysis. Comparisons of short-term and long-term prediction results with Olympus downlink measurements at 19.8 GHz are shown and discussed. Finally, in Section V, a model investigation of the statistical relationship between scintillation variance and microwave brightness temperature is carried out.

II. Modeling Scintillation in Intermittent Turbulence

Among the approaches based on meteorological measurements, the model proposed by Tatarskii has been the most used for calculating the refractive-index structure constant C_n^2 in clear air [19]. The Tatarskii model of the microstructure of the refractive index in turbulent flow relates the value of the refractive-index structure constant C_n^2 to the outer scale of turbulence L_o and to the vertical gradient M of refractivity, assuming a statistically stationary regime and a well-developed homogeneous turbulence following the Kolmogorov law [19], [20]. Actually, in the real atmosphere this condition is only seldom met because the clear air may be locally fluctuating between unstable and stable conditions [21]. Measurements of clear-air turbulence have shown that turbulence may be found in thin layers with sharp randomly varying boundaries, strongly related to the wind shear instability, i.e., turbulence exhibits intermittence phenomena [22], [23].

The intermittent nature of turbulence leads to the need for a local stability criterion, which can be introduced by means of the Richardson number R_i, defined as $R_i = B/S$ where B is the atmospheric buoyancy and S is the square wind shear. Only where R_i is less than or equal to the critical Richardson number R_{ic} (equal to 0.25), the stratification is locally unstable and turbulence is developed so that the Tatarskii model could be directly applied. It has been shown that C_n^2 is mainly related to the structure constants of temperature and humidity, i.e., to the their local vertical gradients, and the transverse wind shears [24]. In order to define a random model of C_n^2, the refractive index structure constant may be supposed as a strongly nonlinear function of the outer scale L_o, of the square wind shear S, and of the vertical gradient M of refractivity (i.e., explicitly of the buoyancy B and of the humidity gradient Q) and can be expressed by [22]

$$C_n^2(L_0,\, S,\, M) = a^2 L_0^{4/3} M^2 u(S - S_c) \tag{1}$$

where $a^2 = 2.8$ and $u(S - S_c)$ is the step function centered on the "critical" square shear S_c defined as: $S_c = B/R_{ic}$. The expression of the refractivity vertical gradient is $M = (\xi B + \zeta Q)^2$, being ξ and ζ functions of pressure, temperature and humidity and Q the vertical gradient of specific humidity. Equation (1) describes the intermittence effects on C_n^2, which is statistically characterized by its probability density function $p(C_n^2)$.

A. Mean Value and Variance of Refractive-Index Structure Constant

The substantial lack of small-scale measurements of the statistical distribution of C_n^2 leads one to perform the calculation of the mean value of C_n^2 in four-dimensional space (L_o, S, B, Q). The calculation may be simplified assuming: 1) as first approximation, the refractivity gradient M, the outer scale L_o, and the square wind shear S to be statistically independent of each other; 2) since the relative fluctuations of B about its large-scale mean value are often small with respect to those of S in free atmosphere, the value of S_c to be a constant given by $S_c = \langle B \rangle / R_{ic}$; and 3) the correlation coefficient between B and Q to be equal to ± 1.

Using the above hypotheses and noting that generally $\langle M \rangle^2 \gg \sigma_M^2$, the mean value of C_n^2 (in $m^{-2/3}$) can be expressed as [22]

$$\langle C_n^2 \rangle \cong a^2 L_{0e}^{4/3} F_S \langle M \rangle^2 = a^2 L_{0e}^{4/3} F_S (\xi \langle B \rangle + \zeta \langle Q \rangle)^2 \tag{2}$$

where the effective outer scale L_{oe} and the intermittence factor F_S are defined as

$$L_{0e}^{4/3} = \int_{L_{om}}^{L_{oM}} L_0^{4/3} p(L_o) dL_o \tag{2a}$$

$$F_S = \int_{S_c}^{\infty} p(S)\, dS \tag{2b}$$

where L_{om} and L_{oM} are, respectively, the minimum and the maximum value experimentally found for L_o.

The scarce availability of small-scale observations still gives rise to difficulties in choosing $p(L_o)$ and $p(S)$. Several probability density functions (pdf's) may be assumed for the shear or for the square shear S. If the horizontal components of the wind-shear vector are supposed normally distributed with the same standard deviation, the shear results distributed according to the Rice–Nagakami pdf. The factor L_{oe} may be evaluated assuming, for instance, a uniform value for $p(L_o)$ between L_{om} and L_{oM}. It is worth noting that if there is no intermittence and the turbulence is well-developed and homogeneous, then $p(S) = 0$ for $S < S_c$ and L_o is a constant. In this case, as expected, the factor F_S reduces to one and (2) becomes equal to the Tatarskii expression.

Following the same approach as described above, it is also possible to calculate the variance of the refractive-index structure constant $\sigma_{C_n^2}^2$, i.e.,

$$\sigma_{C_n^2}^2 = \int_0^{\infty} (C_n^2 - \langle C_n^2 \rangle)^2 p(C_n^2)\, dC_n^2 = \langle (C_n^2)^2 \rangle - \langle C_n^2 \rangle^2. \tag{3}$$

Substituting the expression of C_n^2 given in (1) into (3), we can express the term $\langle (C_n^2)^2 \rangle$ of the previous relationship as

$$\langle (C_n^2)^2 \rangle = \int_{-\infty}^{+\infty} \int_{L_{om}}^{L_{oM}} \int_{S_c}^{\infty} (a^2 L_0^{4/3} M^2)^2 p(L_0, S, M) \cdot dS\, dL_0\, dM. \tag{4}$$

Under the same assumptions valid for obtaining (2), results that

$$\begin{aligned} \langle (C_n^2)^2 \rangle &= a^4 F_S (\langle M \rangle^4 + 2\sigma_{M^2}^2 \langle M \rangle^2 + \sigma_{M^2}^4 + \sigma_{M^2}^2) \\ &\quad \cdot \int_{L_{om}}^{L_{oM}} L_0^{8/3} p(L_0)\, dL_0 \\ &\cong a^4 F_S \langle M \rangle^4 L_{0ev}^{8/3} \end{aligned} \tag{5}$$

where the last approximation is allowed considering that $\sigma_{M^2}^2 \ll (\langle M \rangle^4)$ and $\sigma_{M^2}^4 \ll (\langle M \rangle^4)$ and we have defined

$$L_{0ev}^{8/3} = \int_{L_{om}}^{L_{oM}} L_0^{8/3} p(L_0)\, dL_0. \tag{6}$$

Then, substituting (2) and (5) into (3), we obtain the following approximated expression:

$$\sigma_{C_n^2}^2 \cong a^4 (F_S L_{0ev}^{8/3} - F_S^2 L_{0e}^{8/3}) \langle M \rangle^4. \tag{7}$$

The last equation shows that the variance of C_n^2 can be locally evaluated by knowing the meteorological quantities needed for the estimation of the mean value of C_n^2. It is interesting to analyze the implications of (7). If L_o is supposed to be constant and equal to L_{oc} (i.e., $p(L_o) = \delta(L_o - L_{oc})$ with δ the Dirac function), then (7) can be expressed in terms of structure-constant standard deviation $\sigma_{C_n^2}$ as

$$\sigma_{C_n^2} \cong a^2 \sqrt{F_S (1 - F_S)}\, L_{0c}^{4/3} \langle M \rangle^2 \tag{8}$$

which can be also rewritten by using (2) as

$$\sigma_{C_n^2} \cong \sqrt{\frac{(1 - F_S)}{F_S}}\, \langle C_n^2 \rangle. \tag{9}$$

As physically reasonable, the standard deviation of $\sigma_{C_n^2}$ tends to zero as intermittent turbulence tends to vanish (i.e., $F_S = 0$) or turbulence is well developed and homogeneous (i.e., $F_S = 1$). It is worth noting that $\sigma_{C_n^2}$ is less than $\langle C_n^2 \rangle$ for $F_S \geq 0.5$, while the opposite holds for $F_S < 0.5$ when $\langle C_n^2 \rangle$ becomes very small.

B. Evaluation of Log-Amplitude Fluctuation Variance on Slant Paths

The calculation of the amplitude scintillation variance σ_χ^2, i.e., the variance of the log-amplitude fluctuations χ of the received electromagnetic (EM) field, can be carried out by considering σ_χ^2 as a random function of the structure constant given in (2).

If the Taylor "frozen-in" hypothesis assumed and the atmospheric turbulence lies in the inertial subrange of Kolmogorov's spectrum and is intermittent, we can derive the following expression for the mean variance $\langle \sigma_\chi^2 \rangle$ of log-amplitude fluctuations (expressed in decibels [2]) [20]:

$$\langle \sigma_\chi^2 \rangle = 42.9 k_o^{7/6} \int_0^L \langle C_n^2(r) \rangle r^{5/6}\, dr \tag{10}$$

where L is the path length of the plane wave EM radiation through turbulence, k_o is the wave number in vacuum, and r is the path coordinate. Within a horizontally stratified atmosphere and using the expression given in (2), the evaluation of $\langle \sigma_\chi^2 \rangle$, received by a finite size antenna, can be performed by using the following numerical form of (10) [14]

$$\begin{aligned} \langle \sigma_\chi^2 \rangle &= 23.2 G^2 \frac{a^2 k_o^{7/6}}{(\sin \theta)^3} \sum_{i=1}^{m} (H_i^{11/6} - h_i^{11/6}) \\ &\quad \cdot L_{0e}^{4/3}(i) F_S(i) \langle M(i) \rangle^2 \end{aligned} \tag{11}$$

where H_i and h_i are, respectively, the height of the upper and lower extreme of the ith layer of m turbulent layers, within each $\langle C_n^2(i) \rangle$ is constant, θ is the elevation angle above the surface, and G is the antenna aperture averaging factor (e.g., see [10] and [11]). The mean temporal-power spectrum $\langle W_\chi \rangle$ of log-amplitude fluctuations has a behavior similar to the spectrum in the homogeneous case (characterized by a high-frequency asymptote with logarithmic slope of $-11/3$), but with an area proportional to the mean variance $\langle \sigma_\chi^2 \rangle$.

It is worth mentioning that the use of (10) and (11) can be questionable when dealing with very weak turbulence since in these conditions the inertial subrange of the Kolmogorov spectrum tends to disappear and the spectrum itself might be no more valid. Even generalized scintillation spectra, like those proposed in literature [13], are not applicable because valid only in the case of well-developed turbulence. Since this work was mainly devoted to radiopropagation, the modification of the basic theory of turbulence was beyond our scopes. However, we have tried to parameterized the theory itself in case of very weak turbulence by introducing the intermittence factor F_S [given by (2b)] which modulates in a continuous way the amplitude of scintillation variance, as shown by (11). Ranging from zero to one, the intermittence factor connects the case of laminar flow to that of well-developed turbulence giving an approximation which seems physically reasonable from an EM propagation point of view.

The estimation of $\langle \sigma_\chi^2 \rangle$ can be performed by supposing only one turbulent layer, instead of the multilayer structure assumed in (11). Two simple models can be derived: a slab model where the turbulence layer goes from the surface up to an altitude H and a thin-layer model where the turbulence layer of thickness d goes from an altitude $(H - d)$ up to H being $d \ll H$. From (11) we have for the slab model [20], [25]

$$\langle \sigma_\chi^2 \rangle = 42.3 G^2 \langle C_n^2 \rangle k_0^{7/6} H^{11/6} (\sin \theta)^{11/6} \tag{12a}$$

while for the thin-layer model [25]:

$$\langle \sigma_\chi^2 \rangle = 42.3 G^2 \langle C_n^2 \rangle k_0^{7/6}\, d^{7/3} H^{11/6} (\sin \theta)^{11/6}. \tag{12b}$$

The above expressions given in (11), (12a), and (12b) will be compared in the next sections.

III. Simulating Scintillation from Radio-Sounding Data

The applicability of the expressions given in (2) and (7) requires at least the knowledge of the variability range of L_o, the mean values and the standard deviations of S, B, and Q from small-scale meteorological data sets. An estimate of $\langle C_n^2 \rangle$ is possible if we consider an atmospheric layer defined by two RAOB measurements at two adjacent altitudes and approximate the mean values of meteorological parameters through their spatial averages within the slab. Furthermore, the fluctuations of M and S about their spatial averages are generally small and may be expressed in terms of the spatial averages themselves [22]. Thus, for a specific RAOB we can carry out an estimation of $\langle C_n^2 \rangle$ evaluating the mean values of meteorological variables and their gradients through the spatial averages of RAOB data. In this context the $p(C_n^2)$ assumes the meaning of probability density of occurrence of a given turbulence within the considered slab and $\langle C_n^2 \rangle$ is intended as a slab spatial-average.

We have examined a data set of RAOB's with a vertical spatial resolution of about 250 m or smaller, performed in Milan, Italy by Service Meteorologico Aeronautica Militare Italiana between January 1980 and December 1989. Two radio soundings per day at midday and at midnight have been available for a total of 3655 RAOB's (900, 1025, 840, and 890 samples for spring, summer, autumn, and winter, respectively, while 1800 and 1865 samples for midday and midnight, respectively). An accurate selection of the clear-sky RAOB's has been carried out in order to exclude cloudy and rainy conditions. Linear interpolation procedures have been applied in order to overcome the lack of data at certain levels. The data set has been classified with respect to the hour (midday or midnight), month and season of the balloon launch.

Any result obtained by using the above RAOB data set will be biased by the location and period of acquisition of the data set itself. In particular, the applicability of the proposed prediction methods from meteorological data should be restricted to climates of subcontinental mid-latitude type.

A. Comparison of Scintillation Models

The contribution of each layer to the profile of $\langle C_n^2 \rangle$ and to the total received power $\langle \sigma_\chi^2 \rangle$ can be examined by plotting against the altitude each term of the sum in (11). This analysis is instructive since it gives the physical basis of the statistical results shown in the next sections.

The top-left panel of Fig. 1 shows the vertical profile of the measured temperature T and Richardson number R_i for the RAOB of August 6, 1989 at midday (summer case). Two very stable layers are apparent close to the surface and between 1500 and 3000 m (where $R_i \gg 0.25$), while a well-developed turbulent region is clearly shown between 200 and 1500 m (where $R_i < 0.25$). For altitudes greater than 3000-m turbulence is present with intermediate strength; note that around 3000-m temperature exhibits a thermal inversion corresponding to a high value of R_i. The top-right panel shows the profile of the intermittence factor F_S as derived from (2b): it is close to zero in correspondence with the very stable layers close to the surface and between 1500–3000 m, while close to one within the strong turbulent region between 200–1500 m.

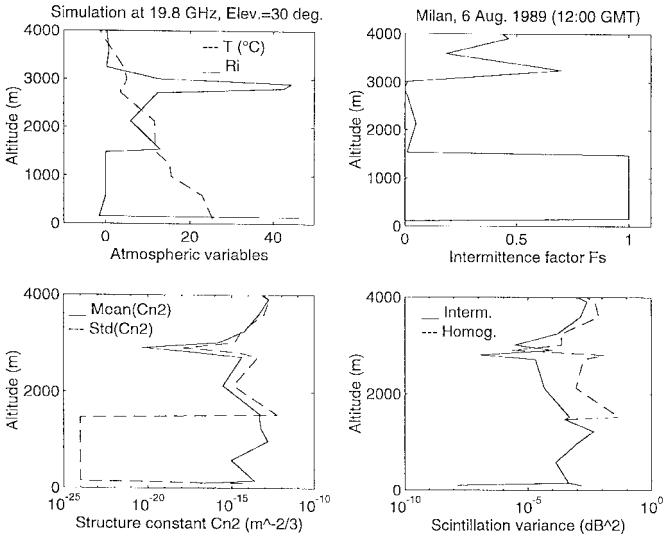

Fig. 1. Simulation from RAOB of August 6, 1989 at midday in Milan. Vertical profile of temperature T and Richardson number R_i (top-left). Profile of the intermittence factor (top-right). Profiles of the mean and standard deviation of C_n^2 (bottom-left). Vertical profile of scintillation variance contribution at 19.8 GHz and 30.6° elevation angle; the solid line refers to the intermittent-turbulence model, while the dashed line indicates the homogeneous-turbulence model (bottom-right).

The bottom-left panel of Fig. 1 shows the profiles of the mean and standard deviation of C_n^2, as calculated from (2) and (11). The mean value $\langle C_n^2 \rangle$ has a minimum around 3200 m where the thermal inversion takes play, while the standard deviation $\sigma_{C_n^2}$ is always slightly greater than $\langle C_n^2 \rangle$ except for the stable regions where $F_S > 0.5$ [see (9)]. Finally, the bottom-right panel shows the vertical profile of the scintillation variance contributions $\langle \sigma_\chi^2(i) \rangle$ of the ith layer, as computed from (11) and indicated by a solid line (intermittent-turbulence model). The area under the $\langle \sigma_\chi^2(i) \rangle$ profile represents the mean received scintillation power $\langle \sigma_\chi^2 \rangle$, which is equal to 1.307 $\times$ 10^{-2} dB^2 in this case. For comparison the dashed line indicates the scintillation variance profile computed by using the formula for $\langle C_n^2 \rangle$ with $F_S = 1$ in (2) (homogeneous-turbulence model). The mean variance of the homogeneous-turbulence model is equal to $\langle \sigma_\chi^2 \rangle = 9.923 \times 10^{-2}$ dB^2, which is higher than the intermittent-turbulence model. This is simply explained by noting that the intermittence factor is much less than one within the two mentioned stable layers.

A very debated issue in literature is the choice of the top level of the turbulent slab or layer [25], [26]. Since it has been shown that the state of turbulence is mainly correlated to the humidity profile [9], we have chosen to truncate the vertical profiles at the height where the water vapor content was less than 0.001 g/m^3. This has lead to the introduction of a height H_t, which indicates the maximum height below which the atmosphere may be either unstable or stable. In the intermittent-turbulence model, this means that the effective turbulent atmosphere will be equal or less than H_t depending on intermittence. Thus, a rough estimation of the turbulence effective height H_{te} can be given by weighting H_t with the

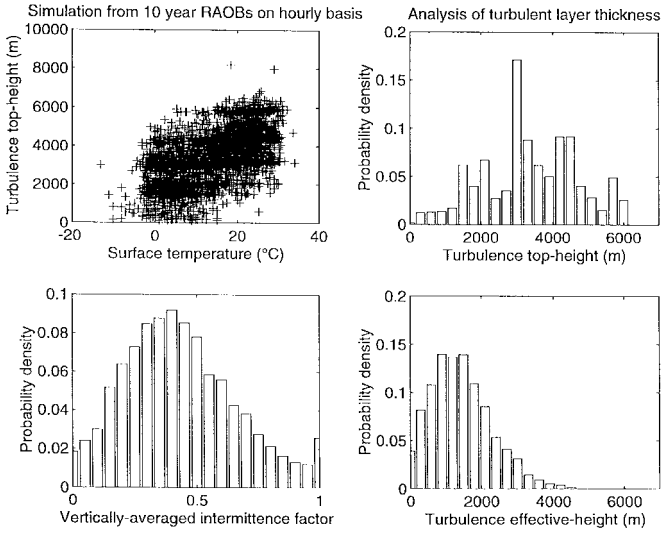

Fig. 2. Analysis of turbulence layer thickness from ten-year RAOB data set. Turbulence top-height H_t as function of surface temperature (top-left). Histogram of turbulence top-height H_t (top-right panel). Histogram of vertically-average intermittence factor F_S (bottom-left panel). Histogram of turbulence effective-height H_{te} (bottom-right panel).

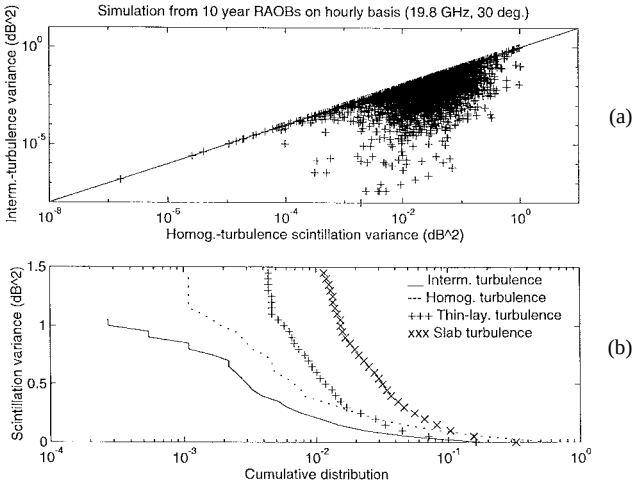

Fig. 3. (a) Comparison of simulated scintillation variances obtained from the intermittent-turbulence model and homogeneous-turbulence model. (b) Comparison of cumulative distribution functions derived from the intermittent-turbulence, the homogeneous-turbulence, the turbulence thin-layer, and the turbulence slab models.

vertically averaged value F_{Sva} of the intermittence factor, i.e.,

$$H_{te} = H_t F_{Sva}. \tag{13}$$

Fig. 2 shows the analysis of turbulence layer thickness derived from the ten-year RAOB data set. The right- and left-top panels show the correlation of H_t with the surface temperature T_S and the histogram of H_t over ten years, respectively. The bottom-left panel shows the histogram of F_{Sva}, while on the right, the histogram of H_{te}, as derived from (13). All the figures refer to data on an hourly basis, without distinguishing season and launch time. A large dispersion of data is noted in the scatterplot, even though the correlation of H_t with T_S is greater than 0.55. The mean value of H is 3380 m and its standard deviation of 1332 m, while the mean value of F_{Sva} is 0.43 with standard deviation of 0.23. The range of H_{te} values, characterized by a mean and standard deviation of 1422 and 845 m, respectively, is in a fairly good agreement with the results shown in [25] and [26] and also in [10] (where they suggest a path length of 2000 m).

Using a given RAOB, we have already showed in Fig. 1 the differences between the intermittent and homogeneous turbulence models and their impact on $\langle\sigma_\chi^2\rangle$ evaluation. The top panel of Fig. 3 illustrates the scatterplot of the scintillation variances derived from the homogeneous and intermittent turbulence models using the whole ten-year data set. Note that the mean value of the difference between the intermittent and homogeneous turbulence model results is -0.0954 dB^2, while its standard deviation is 0.0837 dB^2. The fact that F_S is generally less than one explains the lower values of intermittent-turbulence $\langle\sigma_\chi^2\rangle$ with respect to the homogeneous turbulence results.

The bottom of Fig. 3 shows the cumulative distribution function (CDF) of $\langle\sigma_\chi^2\rangle$ obtained from the whole data set by applying the intermittent-turbulence model [from (11)], the homogeneous-turbulence model [from (11) with $F_S = 1$], the slab-turbulence model [from (12a)] and the thin-layer turbulence model [from (12b)]. For the slab- and thin-layer models we have used the vertical average of $\langle C_n^2\rangle$ profile derived from RAOB's, thus also including the intermittence effects; the slab-top height has been made equal to H_{te} (see Fig. 2), while $d = 400$ m is the chosen thickness of the thin layer. Under these assumptions, both the slab- and thin-layer models tend to overestimate the homogeneous turbulence model results, whose values, in turn, are higher than those of the intermittent turbulence model. In particular, the slab-model results are higher than those of the thin layer, as guessed.

B. Statistical Distribution of Scintillation Parameters

The availability of the RAOB data set can be exploited to infer the statistical distribution of scintillation parameters, like $\langle C_n^2\rangle$ and $\langle\sigma_\chi^2\rangle$. In order to resume the main statistical features, we have performed the vertical average of $\langle C_n^2\rangle$ for each RAOB so that in the following we will refer to its vertically averaged value, indicated by $\langle C_n^2\rangle_{va}$. We will also show simulation results on an hourly basis, that are taking each available RAOB during the day, grouped with respect to hour, month, and season. No particular trends have been noticed by analyzing the interannual variability. Considering the ascending time of a radio-sounding balloon, the evaluation of $\langle\sigma_\chi^2\rangle$ could correspond to the temporal averaging of about 10-min intervals, a period which is comparable to those experimentally used for long-term analysis [25]. Strictly speaking, we have only two samples (midday and midnight) to make our statistics on an hourly basis: the temporal sampling of radio-sounding launches represents a limit of this approach. However, it is important to stress that over the last years the national meteorological agencies have started to perform routinely four RAOB's per day, apart from several scientific campaigns performing radio-soundings.

Fig. 4 shows the histograms of $\langle C_n^2\rangle_{va}$ and $\langle\sigma_\chi^2\rangle$ expressed in logarithmic scale, grouping the ten-year RAOB data set with

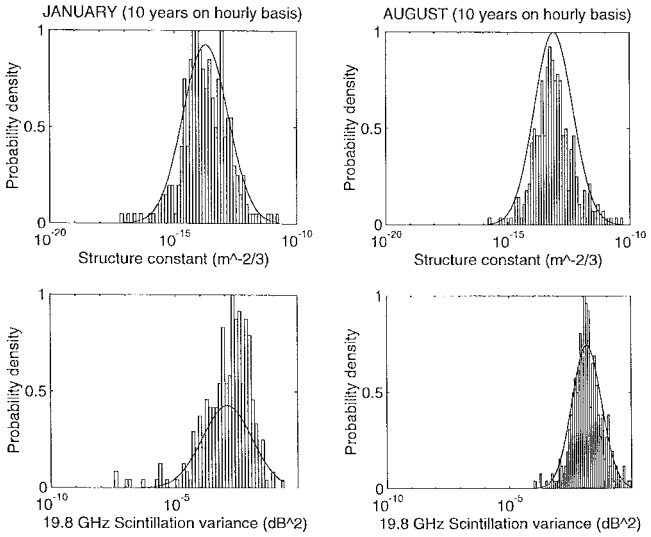

Fig. 4. Histograms of the vertically averaged mean structure constant $\langle C_n^2 \rangle_{va}$ (top panels) and of the scintillation mean variance $\langle \sigma_\chi^2 \rangle$ at 19.8 GHz and 30.6° elevation angle (bottom panels) obtained from the ten-year RAOB data set on an hourly basis with respect to month (only January and August are shown). Histogram intervals are linear on logarithmic scale; best-fitting normal pdf is also indicated by solid line.

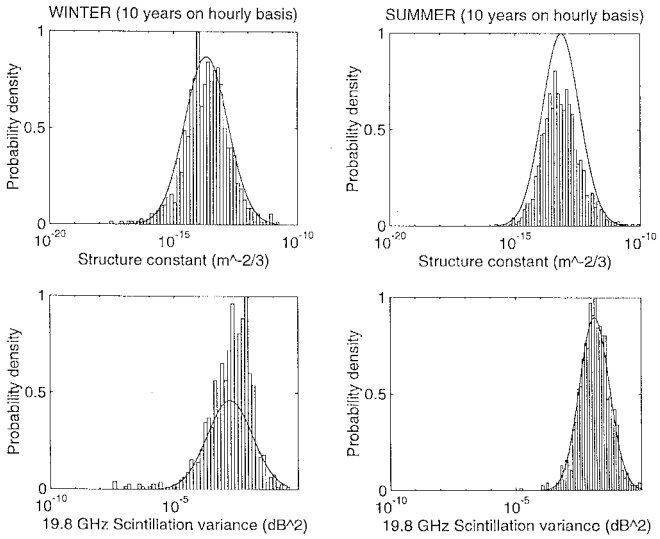

Fig. 5. Same as for Fig. 4, but for data set classified with respect to season (only winter and summer are shown).

respect to month; only the months of January (297 samples) and August (344 samples) are shown. The normal pdf is also shown on each graph by a solid line; a normalization procedure has been necessary to make the comparison on the same plot by imposing the pdf area to be unitary. The normal pdf has resulted to be the best-fitting pdf among the considered ones (in particular, the Γ distribution, the Rayleigh distribution, and the Rice distribution) after performing a χ-square statistical test. Indeed, all the simulated histograms show no noticeable skewness so that it is fairly reasonable to adopt a symmetric distribution on a logarithmic scale. This means that both $\langle C_n^2 \rangle_{va}$ and $\langle \sigma_\chi^2 \rangle$ distribution are well approximated by a log-normal pdf on a linear scale (dB^2 and m$^{-2/3}$, respectively).

In January, the mean value (standard deviation) of $\langle C_n^2 \rangle_{va}$ and $\langle \sigma_\chi^2 \rangle$ is 2.02×10^{-13} m$^{-2/3}$ (1.17×10^{-12} m$^{-2/3}$) and 5.97×10^{-3} dB^2 (1.64×10^{-2} dB^2), respectively; in August it is 6.24×10^{-13} m$^{-2/3}$ (3.09×10^{-12} m$^{-2/3}$) and 4.02×10^{-2} dB^2 (9.58×10^{-2} dB^2), respectively. As expected, the mean values and standard deviations in January are always less than those in August (for $\langle \sigma_\chi^2 \rangle$ up to one order of magnitude). Note that the mean values are generally less at midnight than at midday, while the opposite happens for the standard deviations.

Fig. 5 shows the same as in Fig. 4, but grouping the ten-year RAOB data set with respect to season; only winter (890 samples) and summer (1025 samples) seasons are shown. It is worth noting the fairly good fitting of summer's histogram of $\langle \sigma_\chi^2 \rangle$ by normal pdf as an effect of restricting the grouping criterion, that is selecting more homogeneously the RAOB data set.

In winter the mean value (standard deviation) of $\langle C_n^2 \rangle_{va}$ and $\langle \sigma_\chi^2 \rangle$ is 1.68×10^{-13} m$^{-2/3}$ (8.88×10^{-13} m$^{-2/3}$) and 7.20×10^{-3} dB^2 (2.05×10^{-2} dB^2), respectively; in summer it is 5.08×10^{-13} m$^{-2/3}$ (3.34×10^{-12} m$^{-2/3}$) and 3.40×10^{-2} dB^2 (7.45 dB^2), respectively. The mean values and standard deviations in winter are always less than those in summer; note that summer $\langle C_n^2 \rangle_{va}$ and $\langle \sigma_\chi^2 \rangle$ values are in a fairly good agreement with those published in [13].

From the analysis of Figs. 4 and 5 we can conclude that the best-fitting long-term pdf of $\langle \sigma_\chi^2 \rangle$ (and also $\langle C_n^2 \rangle$) is log-normal on month, season, and year time periods analyzed on an hourly basis. This conclusion is agreement with several experimental results, performed along satellite links with different angles and frequency bands [6], [12], [25]. Thus, we can model $\langle \sigma_\chi^2 \rangle$ pdf as follows:

$$p(\langle \sigma_\chi^2 \rangle) = \frac{1}{\sqrt{2\pi s_\sigma^2} \langle \sigma_\chi^2 \rangle} \exp\left[-\frac{(\ln \langle \sigma_\chi^2 \rangle - m_\sigma)^2}{2 s_\sigma^2} \right] \tag{14}$$

where m_σ and s_σ are the mean and the standard deviation of $\ln(\langle \sigma_\chi^2 \rangle)$, respectively. Hereafter we will refer to $\ln(\langle \sigma_\chi^2 \rangle)$ as scintillation log-variance, expressed conventionally in Np (when $\langle \sigma_\chi^2 \rangle$ is in dB^2). The knowledge of the two statistical moments m_σ and s_σ completely characterized the $\langle \sigma_\chi^2 \rangle$ distribution and the goal of the next section will be to relate them statistically to meteorological parameters. Moreover, (14) allows us to derive the pdf of mean log-amplitude fluctuations $\langle \chi \rangle$ on long-term periods as a marginal pdf of the joined pdf $p(\langle \chi \rangle, \langle \sigma_\chi^2 \rangle)$, i.e., [10]

$$\begin{aligned} p(\langle \chi \rangle) &= \int_0^\infty p(\langle \chi \rangle, \langle \sigma_\chi^2 \rangle)\, d\langle \sigma_\chi^2 \rangle \\ &= \int_0^\infty p(\langle \chi \rangle | \langle \sigma_\chi^2 \rangle) p(\langle \sigma_\chi^2 \rangle)\, d\langle \sigma_\chi^2 \rangle \end{aligned} \tag{15}$$

where $p(\langle \chi \rangle | \langle \sigma_\chi^2 \rangle)$ is the short-term conditional pdf of $\langle \chi \rangle$, introduced through the Bayes theorem. Notice that in (14) and (15) the angle-brackets refer to the ensemble average of small-scale intermittent turbulence phenomena.

There is a substantial consensus in literature to assume $p(\langle \chi \rangle | \langle \sigma_\chi^2 \rangle)$ as Gaussian under statistically stationary conditions on short-term periods that is on what we have called an hourly basis (order of tens of minutes or less). Even though

the scintillation variance can be treated as constant for a short term, it does vary with meteorological conditions. Thus, it is of much interest to infer $\langle\sigma_\chi^2\rangle$ from meteorological data not only on a monthly basis, but also on an hourly basis; this will be another aim of Section IV.

IV. Predicting Scintillation from Surface Meteorological Data

Most of scintillation measurements at ground receiving stations are performed together with surface meteorological measurements such as temperature, relative humidity, and wind velocity. The facility of doing radio soundings close to the satellite ground station is not always planned and more often it is necessary to refer to the closest official RAOB station, which can be many hundreds of kilometers far apart.

Using the statistical multivariate regression method, we have developed several prediction models of amplitude scintillation variance based on the combination of surface temperature and relative humidity. In order to establish the estimation accuracy, we have performed both simulated and experimental tests. As a simulated "truth," we have used the scintillation variances obtained from the corresponding RAOB profiles. The experimental validation of the prediction models has been carried out by using six months of Olympus satellite measurements, sampled around midday and midnight.

In order to make the estimation method independent of antenna-aperture averaging, frequency, and elevation angle, and having in mind the expression (12a), we have introduced a normalized mean scintillation variance as follows:

$$\langle\sigma_\chi^2\rangle_n = \frac{\langle\sigma_\chi^2\rangle}{G^2 f^\alpha (\sin\theta)^{-\beta}} \tag{16}$$

where α and β are the frequency scaling exponent and the elevation scaling exponent, respectively. Following the Tatarskii theory, results that $\alpha = 7/6 = 1.16$ and $\beta = 11/6 = 1.83$ [see (12a)], while in [10] $\alpha = 0.90$ and $\beta = 2.60$, in [11] $\alpha = 1.16$ and $\beta = 2.40$, and in [12] $\alpha = 1.21$ and $\beta = 2.40$. Consistently with the theoretical framework of (10), within our simulation we have chosen the Tatarskii values for α and β. Note that the introduction of $\langle\sigma_\chi^2\rangle_n$ follows the same approach presented in [10] and [12]. The antenna averaging factor G has been assumed to be that suggested by ITU-R [11].

Referring to log-normal pdf of the scintillation log-variance given in (14), the normalization given in (16) implies that

$$m_{\sigma n} = \overline{\ln\langle\sigma_\chi^2\rangle}_n = m_\sigma + \ln\left(\frac{1}{G^2 f^\alpha (\sin\theta)^{-\beta}}\right) \tag{17}$$

where $m_{\sigma n}$ is the mean of normalized scintillation log-variance and the overbar stands for long-term temporal average. It is easy to show that for the standard deviation $s_{\sigma n}$ of normalized scintillation log-variance holds $s_{\sigma n} = s_\sigma$.

A. Scintillation Variance and Surface Meteorological Data

The long-term correlation between the scintillation variance and surface meteorological parameters has been widely exploited, mostly using experimental data [2], [10], [12]. In this section, we will illustrate the results obtained from our simulation in view of developing a prediction model based on ground-based measurements only.

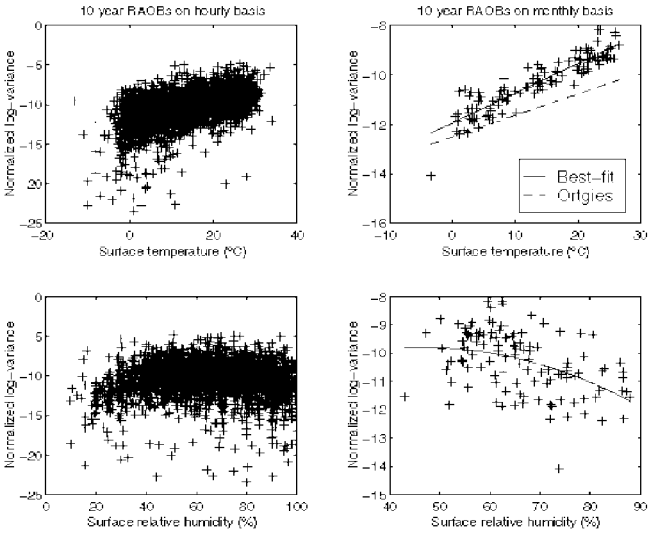

Fig. 6. Normalized scintillation log-variance ($\ln\langle\sigma_\chi^2\rangle_n$) on an hourly basis (left panels) and on a monthly basis (right panels) with surface temperature (top panels) and surface relative humidity (bottom panels), derived from the ten-year RAOB data set. On right panels, best-fitting curve (solid line) and Ortgies's estimation (dashed line [12]) are also indicated.

Fig. 6 shows the normalized log-variance on an hourly basis [i.e., $\ln\langle\sigma_\chi^2\rangle_n$ from (16)] on left panels and on a monthly basis [i.e., $m_{\sigma n}$ from (17)] on right panels against the surface temperature T_S (top panels) and surface relative humidity RH_S (bottom panels) obtained from the ten-year RAOB data set. We show the results on an hourly basis in terms of $\ln\langle\sigma_\chi^2\rangle_n$ and not $\langle\sigma_\chi^2\rangle_n$ since the correlation with surface data is generally much higher. A monthly-basis average means that the simulated scintillation parameters associated to each RAOB and surface data have been temporally averaged over a month.

The (linear) correlation between log-variance and T_S goes from 0.51 on an hourly basis to 0.91 on a monthly basis, while the correlation between log-variance and RH_S goes from -0.02 to -0.43. Thus, the temporal averaging strongly increases the (linear) correlation between log-variance and each surface variable. This effect it is not related to the specific data set considered in this work, but is relative to a more general conclusion obtained from the statistical analysis of temporal series [27]. The general statement is that enlarging the time window, in order to average the samples of two considered random variables, gives rise to an asymptotic increase of the correlation coefficient. Moreover, since in our case there is also a reduction of data variances when passing from an hourly to a monthly basis, this effect is further amplified due to inverse relation between the variance and the correlation coefficient.

The relation between log-variance and RH_S is basically nonlinear and the quadratic best fitting between $m_{\sigma n}$ and RH_S, showed by a solid line in the right-bottom panel, yields

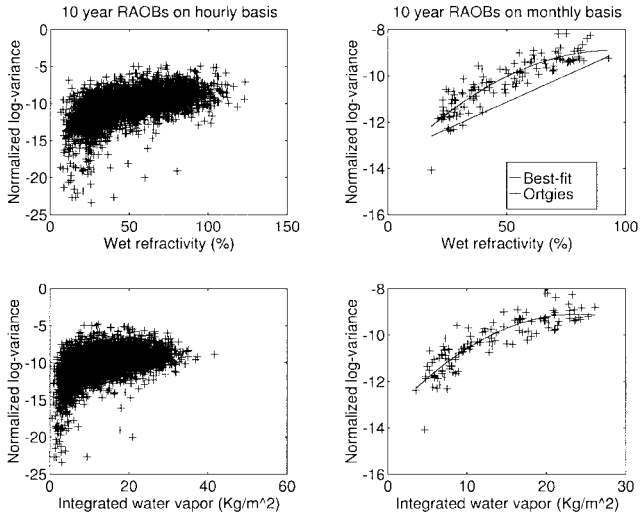

Fig. 7. Same as for Fig. 6, but as function of surface wet refractivity (top panels) and vertically integrated water vapor content (bottom panels).

$m_{\sigma n} = -12.3471 + 0.1079\,\mathrm{RH}_S - 0.0011\,\mathrm{RH}_S^2$. Note that RH_S results negatively correlated both with $\ln\langle\sigma_\chi^2\rangle$ and T_S. This mutual behavior in clear air is related to the strong influence of temperature on scintillation, and indirectly on relative humidity and wind velocity [28]. Due to the solar heating of ground, a layer of warm air results at the earth's surface so that increasing the surface air temperature and producing instability and scintillation. In these cases (and neglecting the impact of humid air masses), there is generally a decrease in relative humidity due to the warmer air being able to hold more moisture (thus increasing the saturated water-vapor pressure). Indeed, after solar heating, the absolute air humidity tends to increase, as shown in [9].

On the top-right panel we also show the linear relationship between $m_{\sigma n}$ and T_S, reported by Ortgies in [12] and indicated by a dashed line. For comparison, the solid line on the same plot indicates the linear best fitting of simulated data (given by $m_{\sigma n} = -11.9419 + 0.1202\ T_S$). The discrepancy may be possibly attributed to different climate conditions used to derive the two relationships.

Fig. 7 shows the same as Fig. 6, but for normalized log-variance against surface-wet refractivity N_{WS} (calculated as indicated in [10]) and vertically integrated water vapor content V_C. The (linear) correlation between log-variance and N_{WS} goes from 0.44 on an hourly basis to 0.82 on a monthly basis, while the correlation between log-variance and V_C goes from 0.44 to 0.82. It is interesting to observe that the correlation $N_{WS} - T_S$ and $V_C - T_S$ are 0.81 and 0.78 on an hourly basis and 0.94 and 0.94 on a monthly basis, respectively. From this figure emerges the importance of knowing V_C to estimate the mean scintillation variance, as will be pointed out in Section V. The quadratic best fitting between $m_{\sigma n}$ and V_C, showed by a solid line in the right-bottom panel, yields $m_{\sigma n} = -13.5103 + 0.3683\ V_C - 0.0027\ V_C^2$.

Again, on the top-right panel we show the linear relationship between $m_{\sigma n}$ and N_{WS} reported by Ortgies in [12] and indicated by a dashed line. For comparison, the solid line on the same plot indicates the quadratic best fitting of simulated data (given by $m_{\sigma n} = -13.9393 + 0.1059\ N_{WS} - 0.0006\ N_{WS}^2$). The Ortgies predicted values are lower than those estimated by the best-fitting curve (note that the correction due to the quadratic term N_{WS}^2 is very small).

TABLE I
COMPARISON OF STATISTICAL REGRESSION METHODS TO ESTIMATE THE NORMALIZED LOG VARIANCES ON AN HOURLY BASIS [I.E., $\ln\langle\sigma_\chi^2\rangle_n$ GIVEN IN (16)] AND ON A MONTHLY BASIS [I.E., $m_{\sigma n}$ GIVEN IN (17)] FROM SURFACE METEOROLOGICAL VARIABLES, OBTAINED BY USING THE TEN-YEAR TRAINING DATA SET. THE VARIOUS POLYNOMIAL FORMS ARE COMPARED IN TERMS OF RMS ERROR, CORRELATION COEFFICIENT, AND GAIN RATIO (RATIO BETWEEN TRAINING AND ESTIMATE RMS ERRORS)

		HOURLY BASIS			*MONTHLY BASIS*		
Predictors		**rms error**	**correlation**	**gain ratio**	**rms error**	**correlation**	**gain ratio**
T_S	*linear*	1.6767	0.5626	1.2096	0.4531	0.8782	2.0906
N_{WS}	*linear*	1.7152	0.5337	1.1825	0.4831	0.8602	1.9607
T_S-RH_S	*linear*	1.6777	0.5619	1.2089	0.4445	0.8830	2.1307
T_S- N_{WS}	*linear*	1.6918	0.5516	1.1989	0.4408	0.8851	2.1487
T_S	*quadratic*	1.7322	0.5202	1.1709	0.4548	0.8772	2.0826
N_{WS}	*quadratic*	1.6780	0.5617	1.2087	0.4705	0.8679	2.0131
T_S-RH_S	*quadratic*	1.6435	0.5854	1.2334	0.4302	0.8857	2.1540
T_S-N_{WS}	*quadratic*	1.6607	0.5733	1.2205	0.4334	0.8842	2.1411

B. Multivariate Estimation of Scintillation Parameters

In order to estimate $\ln\langle\sigma_\chi^2\rangle_n$ on an hourly basis and $m_{\sigma n}$ on a monthly basis, we have tested several regression models both linear and quadratic, selecting as predictors various combination of T_S, RH_S, and N_{WS}. We have also tried a stepwise regression, but without significant improvements with respect to global regression results. As a simulated test data set, we have used one-fifth (731 samples) of the whole ten-year data set on both an hourly and a monthly basis, using the remaining observations (2924 samples) as a training data set.

The estimation results of the simulated test are shown in Table I in terms of root mean square (rms) error, correlation coefficient, and gain ratio. The last quantity expresses the ratio between the training-set standard deviation and the estimate rms error; thus, it should be as much greater than one as possible to select the best estimator. With the aim of making the test more realistic (and robust to noise), we have added to the simulated test measurements a Gaussian noise of zero mean and standard deviation equal to 1% of the value itself. Note that we have not included the mixed terms in the quadratic form.

The analysis of Table I results shows that the best regressive estimators are the one based on surface temperature and humidity in quadratic form (STH2), and the one based on surface temperature and wet refractivity in quadratic form (STN2). It is worth mentioning that most of the prediction algorithms proposed in literature give formulas based on either temperature or wet-refractivity in linear form [6], [10], [12]. Table I shows that a linear relationship is actually proper only for temperature-based predictors, while quadratic estimators using mix meteorological data generally have better performances. The STH2 and STN2 methods have the following expression on an hourly basis:

$$\langle\sigma_\chi^2\rangle_n = \exp(a_{01} + a_{11}\,T_s + a_{21}\,\mathrm{RH}_s + a_{31}\,T_s^2 + a_{41}\,\mathrm{RH}_s^2) \tag{18a}$$

$$\langle\sigma_\chi^2\rangle_n = \exp(a_{02} + a_{12}\,T_s + a_{22}\,N_{WS} + a_{32}\,T_s^2 + a_{42}\,N_{WS}^2) \tag{18b}$$

TABLE II
REGRESSION COEFFICIENTS OF (18) AND (19) AND ASSOCIATED RMS ERROR GIVEN IN Np FOR $\ln\langle\sigma_\chi^2\rangle_n$ AND $\ln\langle C_n^2\rangle_{va}$ AND IN m FOR H_{te} AND OBTAINED BY USING THE TEN-YEAR TRAINING DATA SET. NOTE THAT T_S IS EXPRESSED IN °C, RH_S IN % AND N_{WS} IN %

	HOURLY BASIS					
Equation	**coef_0**	**coef_1**	**coef_2**	**coef_3**	**coef_4**	**rmse**
(18a)	-16.6602	0.1796	0.1192	-0.0018	-0.0007	1.6435 Np
(18b)	-13.8732	0.0771	0.0875	-0.0014	-0.0005	1.6607 Np
	MONTHLY BASIS					
Equation	**coef_0**	**coef_1**	**coef_2**	**coef_3**	**coef_4**	**rmse**
(19a)	-14.9504	0.1546	0.0747	-0.0011	-0.0005	0.4302 Np
(19b)	-12.3889	0.1300	0.0151	-0.0016	0.0000	0.4334 Np

while on a monthly basis we have

$$m_{\sigma n} = b_{01} + b_{11}\,T_s + b_{21}\,\mathrm{RH}_s + b_{31}\,T_s^2 + b_{41}\,\mathrm{RH}_s^2 \quad (19a)$$

$$m_{\sigma n} = b_{02} + b_{12}\,T_s + b_{22}\,N_{WS} + b_{32}\,T_s^2 + b_{42}\,N_{WS}^2. \quad (19b)$$

The form of (18) depends on the fact that (as already said) $\ln\langle\sigma_\chi^2\rangle_n$ has resulted more correlated to each predictor set than $\langle\sigma_\chi^2\rangle_n$ on an hourly basis. Table II reports the regression coefficients of (18) and (19), using the whole ten-year data set on an hourly and a monthly basis. These regression coefficients could be specified for any classification of the RAOB data set (e.g., results on a weekly basis are not shown). The above coefficients are valid for any link specifications, when transforming normalized variables through (16) and (17).

Using the simulated test data set on an hourly and a monthly basis, it results that the major differences between STH2 and STN2 algorithms are relative to an hourly basis case where STN2 tends to underestimate high values of $\langle\sigma_\chi^2\rangle_n$; on a monthly basis, the results are fairly good for both methods.

Finally, it can be interesting to provide also the statistical relationships to estimate the vertical average of $\langle C_n^2\rangle_{va}$ and the turbulence effective height H_{te}. Performing tests similar to those described above, we have found the following relationships on an hourly basis:

$$\langle C_n^2\rangle_{va} = \exp(c_{01} + c_{11}\,T_s + c_{21}\,\mathrm{RH}_s + c_{31}\,T_s^2 + c_{41}\,\mathrm{RH}_s^2) \quad (20a)$$

$$\langle C_n^2\rangle_{va} = \exp(c_{02} + c_{12}\,T_s + c_{22}\,N_{WS} + c_{32}\,T_s^2 + c_{42}\,N_{WS}^2) \quad (20b)$$

and

$$H_{te} = d_{01} + d_{11}\,T_s + d_{21}\,\mathrm{RH}_s + d_{31}\,T_s^2 + d_{41}\,\mathrm{RH}_s^2 \quad (21a)$$

$$H_{te} = d_{02} + d_{12}\,T_s + d_{22}\,N_{WS} + d_{32}\,T_s^2 + d_{42}\,N_{WS}^2 \quad (21b)$$

while on a monthly basis we have

$$m_{C_{va}} = e_{01} + e_{11}\,T_s + e_{21}\,\mathrm{RH}_S + e_{31}\,T_S^2 + e_{41}\,\mathrm{RH}_s^2 \quad (22a)$$

$$m_{C_{va}} = e_{02} + e_{12}\,T_S + e_{22}\,N_{WS} + e_{32}\,T_S^2 + e_{42}\,N_{WS}^2 \quad (22b)$$

and

$$\mu_{H_{te}} = g_{01} + g_{11}\,T_S + g_{21}\,\mathrm{RH}_S + g_{31}\,T_S^2 + g_{41}\,\mathrm{RH}_S^2 \quad (23a)$$

$$\mu_{H_{te}} = g_{02} + a_{12}\,T_S + g_{22}\,N_{WS} + g_{32}\,T_S^2 + g_{42}\,N_{WS}^2 \quad (23b)$$

where $m_{C_{va}}$ and $m_{H_{te}}$ are the long-term average (on a monthly basis) of $\ln\langle C_n^2\rangle_{va}$ and H_{te}, respectively.

Table III reports the regression coefficients of (20)–(23), using the whole ten-year data set on an hourly and a monthly basis. On an hourly basis both the estimation of $\ln\langle C_n^2\rangle_{va}$ and H_{te} exhibits a poor correlation, which significantly improves on a monthly basis, especially for H_{te}.

TABLE III
REGRESSION COEFFICIENTS OF (20)–(23) AND ASSOCIATED RMS ERROR GIVEN IN Np FOR $\ln\langle\sigma_\chi^2\rangle_n$ AND $\ln\langle C_n^2\rangle_{va}$ AND IN m FOR H_{te} AND OBTAINED BY USING THE TEN-YEAR TRAINING DATA SET. NOTE THAT T_S IS EXPRESSED IN °C, RH_S IN % AND N_{WS} IN %

	HOURLY BASIS					
Equation	**coef_0**	**coef_1**	**coef_2**	**coef_3**	**coef_4**	**rmse**
(20a)	-34.2705	0.0911	0.0654	-0.0005	-0.0005	1.8156 Np
(20b)	-32.5261	0.0673	0.0201	-0.0007	-0.0001	1.8215 Np
(22a)	1022.5	42.0000	0.7	-0.2	0.0	753.6 m
(22b)	871.3157	52.8218	-1.4805	0.0766	-0.0468	751.5672 m
	MONTHLY BASIS					
Equation	**coef_0**	**coef_1**	**coef_2**	**coef_3**	**coef_4**	**rmse**
(21a)	-33.6086	0.0573	0.0478	0.0006	-0.0003	0.5331 Np
(21b)	-31.1656	0.1057	-0.0449	-0.0015	0.0005	0.5210 Np
(23a)	2.995.3	0.0316	-44.7	0.0	0.2	207.9 m
(23b)	1.720.2	0.0910	-42.0	0.0	0.2	209.4 m

C. Comparison with Olympus Satellite Measurements

In order to validate the above estimation methods, a statistical comparison with Olympus scintillation measurements at 19.8 GHz (namely, 19.77 GHz), acquired at the receiving ground-station in Milan at 30.6° elevation over a period going from July to December 1992, has been performed. The temporal series of scintillation amplitude variance has been provided every one minute after a high-pass filtering of the raw copolar received signal [6]. Clear-air measurements have been carefully selected both by visual inspection and by a threshold on the measured copolar attenuation. Surface meteorological measurements have been available during the Olympus experiment every ten minutes. In order to create a correspondence with RAOB launch time, Olympus measurements around midday and midnight have been screened making an average of 15 min after midday and midnight to match the time needed for the RAOB balloon to complete the ascending path.

Fig. 8 shows the scatterplot between the log-variance of 19.8-GHz Olympus measurements and the log-variance, estimated from (18) and (19) using the simulated test data set on an hourly basis (left panels) and a monthly basis (right panels). Top panels show the results using the STH2 algorithms given in (18a) and (19a), while bottom panels show the results using the STN2 algorithms given in (18b) and (19b). On an hourly basis (left panels) we have 119 samples, while on a monthly basis (right panels) we have only six samples. For comparison, we have also indicated on right panels the long-term estimates performed by applying two algorithms of Ortgies, one using the surface temperature (Ortgies-T) and the other using the surface wet refractivity (Ortgies-N) as predictors in (17), applying the proper coefficients α and β [12].

The rms error on an hourly basis tends generally to increase with higher values of scintillation log-variance, but strongly to decrease when doing temporal averaging. Quantitatively speaking, on an hourly basis the bias and the rms errors are, respectively, 0.1680 and 0.8827 for STH2 algorithm, and 0.2745 and 1.0081 for STN2 algorithm; on a monthly basis, they are −0.0266 and 0.2624 for STH2 algorithm, 0.1086 and 0.3834 for STN2, 0.2239 and 0.7220 for Ortgies-N algorithm, and −0.7624 and 0.3736 for Ortgies-T algorithm. It is worth mentioning that if for STH2 and STN2 algorithms we use the same normalization proposed by Ortgies (i.e., his α and

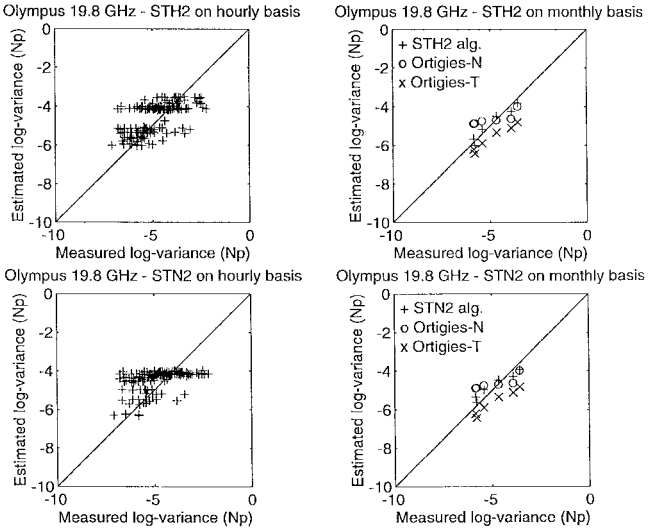

Fig. 8. Olympus measured scintillation log-variance at 19.8 GHz and 30.6° elevation against the estimated log-variance on an hourly basis (left panels) and on a monthly basis (right panels). Top panels refer to STH2 prediction algorithms, while bottom panels to STN2 algorithms. On right panels, Ortgies's estimates based on temperature (Ortgies-T) and wet refractivity (Ortgies-N) are also indicated [12].

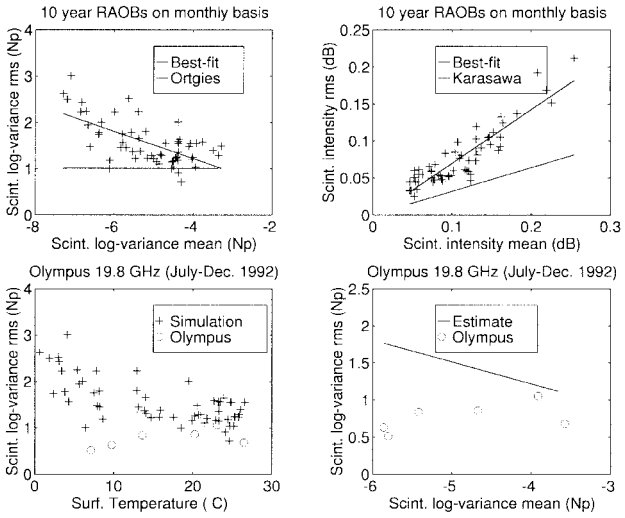

Fig. 9. Analysis of standard deviation of scintillation log-variance s_σ on a monthly basis at 19.8 GHz on 30.6° elevation angle. Simulated s_σ against mean m_σ of scintillation log-variance (top-left); best-fitting curve (solid line) and Ortgies's constant value (dashed line [12]) are also shown. Simulated standard deviation s_σ of scintillation variance against its mean m_σ (top-right); best-fitting curve (solid line) and Karasawa's relationship (dashed line [10]) are also plotted. Simulated and Olympus-derived s_σ against surface temperature (bottom-left). s_σ against m_σ derived from Olympus measurements (bottom-right); estimate of using (24b) is also shown.

β coefficients), then the bias and the rms error become, respectively, 0.4854 and 0.2624 for STH1 and 0.6205 and 0.3834 for STN2.

So far, we have dealt with m_σ, but, as said, the scintillation variance pdf [given in (14)] is also characterized by the standard deviation s_σ of $\ln(\langle\sigma_\chi^2\rangle)$. From experimental data (based on 108 months), Ortgies found values ranging from 0.85 and 1.15, not dependent on frequency and meteorological data; thus, he has assumed $s_\sigma = 1.01$ corresponding to the measured mean value [12]. The results of Karasawa *et al.* [10] cannot be directly compared in terms of s_σ since they adopted a Γ distribution for scintillation intensity $\langle\sigma_\chi\rangle$; the experimental relationship they have proposed is $\sigma_\sigma = 0.32\ \mu_\sigma$, where μ_σ and σ_σ are the long-term mean and standard deviation of $\langle\sigma_\chi\rangle$ [2].

The long-term estimation of s_σ can be also carried out by using the model-based approach. The top panels of Fig. 9 show the scatter plot of simulated s_σ (left panel) and σ_σ (right panel) against m_σ and μ_σ, respectively. For comparison, the experimental relationships of Ortgies and Karasawa *et al.*, are also indicated by dashed lines on the respective plots. From model simulation we can derive the following relationships:

$$s_\sigma = 0.0397 - 0.2948\, m_\sigma \tag{24a}$$

$$\sigma_\sigma = -0.0028 + 0.7254\, \mu_\sigma. \tag{24b}$$

Both (24a) and (24b) give values higher than those predicted by the Ortgies and Karasawa experimental relationships, respectively.

The bottom panels of Fig. 9 show (right panel) the comparison between the simulated and measured s_σ as a function of surface temperature and (left panel) the scatterplot between the measured m_σ and s_σ, where the estimate of s_σ made by (24a) is also indicated. From both simulation and measurements no particular trends with temperature can be observed, a fact in agreement with what was noted by Ortgies [12]. The mean value of simulated s_σ is 1.5323, while that of Olympus measurements is 0.7619, which is below the values observed by Ortgies. The estimate of s_σ gives values between 1.12 and 1.75 and tends to overestimate measured s_σ values especially for small log-variance mean values m_σ. This fact may be due to the undersampling of the Olympus-signal temporal series; that is, to the choice to retain only measurements around midday and midnight. Moreover, this choice can also impact simulation results since we have been forced to neglect the daily evolution of meteorological conditions.

V. Correlating Scintillation and Brightness Temperature

A correlation between scintillation and brightness temperature measurements has been already shown in literature by using experimental data [3], [18]. In this section, we tackle a model investigation in order to include in the prediction methods of amplitude scintillation variance also the measurements of integrated water vapor content. To do this, we have restricted our analysis to the year 1989 of the RAOB data set.

A. Examples of Combined Simulations

At microwave frequencies the tropospheric attenuation is mainly caused by the spectral absorption of water vapor, oxygen and cloud liquid water. Under the assumption of local thermodynamic equilibrium and in the absence of scattering, the thermal emission is expressed in terms of equivalent blackbody brightness temperature T_B using the Rayleigh–Jeans approximation [20]. The T_B can be expressed in terms of total attenuation or optical thickness τ (decibels) using the radiative transfer equation and introducing the mean radiative temper-

ature, which resumes the vertical dependence of atmospheric variables.

In order to simulate the observed T_B by a ground-based microwave radiometer at a given frequency and in a given direction, we have used the Liebe model [29] to characterize the atmospheric absorption. This model gives a detailed description of the spectral molecular absorption of humid air (possibly, with some cloud liquid) in the frequency range from 1 to 1000 GHz as a function of the local temperature, pressure and relative humidity. The radiative transfer equation has been numerically solved by supposing a plane-parallel atmosphere with levels associated to RAOB vertical soundings. At the top boundary, we have assumed an incident radiation equal to cosmic background T_B (about 2.7 K). Since RAOB does not provide cloud liquid water, the radiative transfer algorithm selects its presence at levels where the relative humidity is higher than 90%. However, all RAOB's presenting possible cloud liquid layers have been neglected since the framework of this study is valid under clear-air conditions.

Fig. 10 shows the scintillation log-variances at 18.7, 39.5, and 49.5 GHz (Italsat frequencies) against the 23.8-GHz brightness temperatures on an hourly basis (left panel) and a monthly basis (right panel), both derived from each RAOB of 1989 using a radiative transfer model and the scintillation model with the same elevation and antenna aperture used for 19.8-GHz Olympus simulation. The (linear) correlation coefficients on an hourly basis are of 0.51 for 18.7 GHz, 0.50 for 39.6 GHz, and 0.50 for 49.5 GHz scintillation log-variance, while on a monthly basis they increase to 0.93, 0.92, and 0.92, respectively. As expected, scintillation log-variances increase with frequency (maximum values goes from -4.3905 Np at 18.7 GHz up to -2.5874 Np at 49.5 GHz), even though their dynamic range slightly decrease with frequency (from 2.2469 Np at 18.7 GHz down to 2.1765 Np at 49.5 GHz). This correlation between scintillation variances and downwelling brightness temperatures has a physical explanation. As already said, the solar heating of ground causes an increase of the surface air temperature and absolute humidity with production of instability and scintillation. Since brightness temperature basically represents the thermal radiation of the atmosphere, it is clearly motivated the positive correlation between $\langle \sigma_\chi^2 \rangle$ and T_B.

As expected in clear-air conditions [16], the linear correlation between brightness temperatures at 23.8 GHz and at 31.6 GHz and the integrated water vapor content V_C, is very high (0.99 for 23.8 GHz and 0.98 for 31.6 GHz). The 23.8 GHz T_B exhibits much higher values (up to 120 K in summer) than 31.6 GHz T_B (up to 40 K in summer) due to the fact that 23.8-GHz frequency band is more strongly absorbed by water vapor. These results motivate the use of linear statistical methods to estimate V_C (in kg/m^2) from T_B measurements (in K) in clear-air, i.e.,

$$V_c = v_{01} + v_{11}\, T_{B23} \tag{25a}$$

$$V_C = v_{02} + v_{12}\, T_{B31} \tag{25b}$$

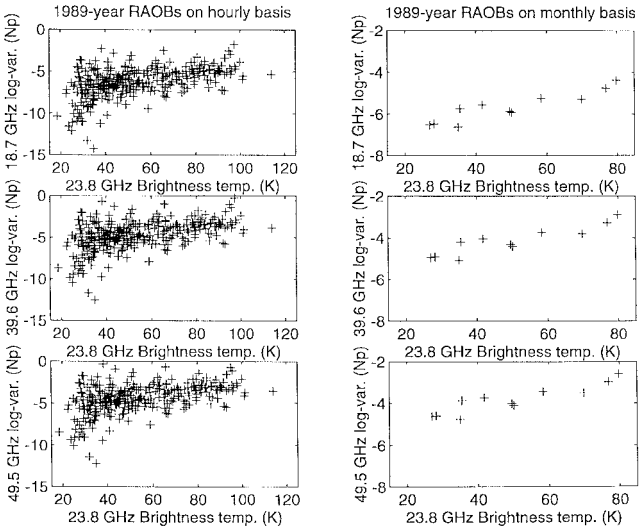

Fig. 10. Simulated scintillation mean variance at Italsat beacon frequencies, i.e., 18.7 GHz (top panels), 39.6 GHz (center panels), and 49.5 GHz (bottom panels), against brightness temperature at 23.8 GHz, derived from the ten-year data set on an hourly basis (left panels) and a monthly basis (right panels).

where T_{B23} and T_{B31} are the brightness temperatures at 23.8 and 31.6 GHz, respectively. On an hourly basis, the regression coefficients of (25a) are given by $v_{01} = -5.2252$ and $v_{11} = 0.3531$ and those of (25b) by $v_{02} = -15.8063$ and $v_{12} = 0.9241$, with an rms error of 0.906 kg/m^2 and 1.032 kg/m^2, respectively. On a monthly basis, the regression coefficients of (25a) are given by $v_{01} = -4.9457$ and $v_{11} = 0.3475$ and those of (25b) by $v_{02} = -15.6446$ and $v_{12} = 0.9189$, with an rms error of 0.241 kg/m^2 and 0.267 kg/m^2, respectively. Due to the small data dispersion and to the linear relationship, the regressions coefficients of (25) on an hourly basis and on a monthly basis are not very different.

The rms error, obtained using the T_B at 31.6 GHz as a predictor, is higher than that using the T_B at 23.8 GHz and it must be also noted that 31.6 GHz T_B is much more sensitive to the cloud liquid–water presence so that in practical applications the errors can be much greater than those expected. In fact, the use of a dual-channels radiometer with a channel around the 22-GHz water-vapor absorption lines and a window-channel around 30–40 GHz is justified by the need of estimating V_C also in presence of cloud liquid water along the path [16]. More general algorithms use both T_B at 23.8 and 31.6 GHz to estimate both integrated water vapor and cloud liquid water contents in order to fulfill the requirement to operate in any weather condition (except precipitation) [17].

B. New Estimation Methods Including Integrated Water Vapor

In the previous paragraph we have demonstrated how integrated water vapor V_C can be derived from T_B measurements. On the other hand, Fig. 7 has shown a good correlation between normalized scintillation log-variance and V_C, so that it is interesting to explore the possibility to estimate $\langle \sigma_\chi^2 \rangle$ from a combination of surface temperature T_S, relative humidity RH_S (or wet refractivity N_{WS}), and integrated water vapor V_C. Thus, by applying the multivariate statistical regression

TABLE IV
REGRESSION COEFFICIENTS OF (26) AND (27) AND ASSOCIATED RMS ERROR (RMSE), GIVEN IN Np FOR $\ln\langle\sigma_\chi^2\rangle_n$ AND $\ln\langle C_n^2\rangle_{va}$ AND IN m FOR H_{te} AND OBTAINED BY USING THE TEN-YEAR TRAINING DATA SET. NOTE THAT T_S IS EXPRESSED IN °C, RH_S IN %, AND V_C IN Kg/m^2

	HOURLY BASIS							
Equation	**coef_0**	**coef_1**	**coef_2**	**coef_3**	**coef_4**	**coef_5**	**coef_6**	**rmse**
(26a)	-16.8224	0.1413	0.1101	0.1337	-0.0009	-0.0007	-0.0040	1.6306 Np
(26b)	-35.5937	0.1681	0.1126	-0.1945	0.0002	-0.0007	0.0024	1.7637 Np
(26c)	1300.4	4.3	-15.9	111.9	0.0	0.0	-2.4	736.2 m
	MONTHLY BASIS							
Equation	**coef_0**	**coef_1**	**coef_2**	**coef_3**	**coef_4**	**coef_5**	**coef_6**	**rmse**
(27a)	-15.0762	0.1473	0.0772	0.0133	-0.0006	-0.0005	-0.0007	0.4297 Np
(27b)	-34.3756	0.1598	0.0994	-0.3443	0.0017	-0.0006	0.0064	0.4721 Np
(27c)	3113.3	18.6	-51.9	45.1	-0.2	0.3	-0.8	205.1 m

method and proceeding in the same way as in Section IV, we have derived the following relationships on an hourly basis:

$$\langle\sigma_\chi^2\rangle_n = \exp(a_{0v} + a_{1v}T_S + a_{2v}\mathrm{RH}_S + a_{3v}V_C + a_{4v}T_S^2 + a_{5v}\mathrm{RH}_S^2 + a_{6v}V_C^2) \quad (26a)$$

$$\langle C_n^2\rangle_{va} = \exp(c_{0v} + c_{1v}T_S + c_{2v}\mathrm{RH}_S + c_{3v}V_C + c_{4v}T_S^2 + c_{5v}\mathrm{RH}_S^2 + c_{6v}V_C^2) \quad (26b)$$

$$H_{te} = e_{0v} + e_{1v}T_S + e_{2v}\mathrm{RH}_S + e_{3v}V_C + e_{4v}T_S^2 + e_{5v}\mathrm{RH}_S^2 + e_{6v}V_C^2 \quad (26c)$$

while on a monthly basis we have

$$m_{\sigma n} = b_{0v} + b_{1v}T_S + b_{2v}\mathrm{RH}_S + b_{3v}V_C + b_{4v}T_S^2 + b_{5v}\mathrm{RH}_S^2 + b_{6v}V_C^2 \quad (27a)$$

$$m_{C_{va}} = d_{0v} + d_{1v}T_S + d_{2v}\mathrm{RH}_S + d_{3v}V_C + d_{4v}T_S^2 + d_{5v}\mathrm{RH}_S^2 + d_{6v}V_C^2 \quad (27b)$$

$$\mu_{H_{te}} = g_{0v} + g_{1v}T_S + g_{2v}\mathrm{RH}_s + g_{3v}V_C + g_{4v}T_{s2} + g_{5v}\mathrm{RH}_S^2 + g_{6v}V_{c2}. \quad (27c)$$

Table IV provides the coefficients of (26) and (27) for the ten-year data set, as in Tables II and III. Equations (26) and (27) have the form of the STH2 algorithm. Formulas having the structure of STN2 algorithm and where V_C is included as a quadratic term are not shown for brevity; in any case, their rms errors are comparable with STH2 algorithm results given in Table IV.

From a comparison of Table IV with Table III, it emerges that the inclusion of V_C among the predictors significantly reduces the rms errors, especially on a monthly basis. These results would encourage the installation of a dual-channel radiometer at satellite beacon receiving stations, not only for attenuation estimates, but also for scintillation studies and applications.

VI. CONCLUSIONS

The intermittence phenomenon in turbulent atmosphere has been modeled by means of a statistical formulation of the homogeneous turbulence structure constant. First- and second-order statistical moments of the structure constant have been computed and a procedure has been described in order to estimate the mean structure constant and received amplitude scintillation variance from RAOB data in clear-air conditions. A RAOB data set, collected in Milan from 1980 to 1989 has allowed us to infer the statistical distribution of the scintillation mean parameters to be used in the gain budget evaluation of satellite microwave links.

The statistical regression method has been applied to the estimation of scintillation parameters (such as variance, structure constant, and turbulence height) from surface meteorological data, proposing coefficient tables valid on a monthly basis and on an hourly basis. A preliminary validation of estimation methods has been carried out using Olympus satellite measurements at 19.8 GHz acquired at Milan ground-station at 30° elevation angle. The comparison results show that the proposed methods are fairly accurate and can be promising tools also for comparison with Italsat data up to 50 GHz.

The possibility of using the measurements of a dual-channel microwave radiometer has been also investigated through a model analysis. The capability of microwave radiometers to provide a fairly good estimation of integrated water vapor has been further assessed. The estimation methods of scintillation parameters have been also extended to include integrated water vapor estimates among the surface statistical predictors, showing the reduction of rms errors when this extension is performed. Even though this model investigation has clearly shown the potential of microwave radiometers for scintillation studies, further experimental validation are needed. Future aspects of this work will include a systematic validation of the obtained results by using Italsat experiment data in the 20–50 GHz frequency range.

ACKNOWLEDGMENT

The authors would like to thank Dr. E. Fionda of Fondazione Ugo Bordoni, Rome, Italy, for his helpful collaboration and one of the anonymous reviewers for his thorough comments. RAOB data have been kindly provided by Servizio Meteorologico Aeronautica Militare Italiana, while Olympus satellite measurements have been made available by Dr. C. Riva of Politecnico di Milano, Milan, Italy.

REFERENCES

[1] O. P. Banjo and E. Vilar, "Measurements and modeling of amplitude scintillations on low-elevation Earth-space paths and impact on communication systems," *IEEE Trans. Commun.*, vol. COM-34, pp. 774–780, Aug. 1986.
[2] Y. Karasawa, K. Yasukawa, and M. Yamada, "Tropospheric scintillation in the 14/11-GHz bands on earth-space paths with low elevation angles," *IEEE Trans. Antennas Propagat.*, vol. 36, pp. 563–569, Apr. 1988.
[3] P. Basili, G. d'Auria, P. Ciotti, P. Ferrazzoli, and D. Solimini, "Case study of intense scintillations along the OTS space-earth link," *IEEE Trans. Antennas Propagat.*, vol. 38, pp. 107–113, Jan. 1990.
[4] E. T. Salonen, J. K. Tervonen, and W. J. Vogel, "Scintillation effects on total fade distributions for earth-satellite links," *IEEE Trans. Antennas Propagat.*, vol. 44, pp. 1–5, Jan. 1996.
[5] E. Matricciani, M. Mauri, and C. Riva, "Relationship between scintillation and rain attenuation at 19.77 GHz," *Radio Sci.*, vol. 31, no. 2, pp. 273–279, 1996.
[6] G. Peeters, F. S. Marzano, G. d'Auria, C. Riva, and D. Vanhoenacker-Janvier, "Evaluation of statistical prediction models for clear-air scintillation using Olympus satellite measurements," *Int. J. Sat. Commun.*, vol. 15, pp. 73–88, 1997.
[7] M. Filip and E. Vilar, "Optimum utilization of the channel capacity of a satellite link in the presence of amplitude scintillations and rain attenuation," *IEEE Trans. Commun.*, vol. COM-28, pp. 1958–1965, Nov. 1990.
[8] G. De Angelis, A. Paraboni, C. Riva, F. Zaccarini, G. Dellagiacoma, L. Ordano, R. Polonio, M. Mauri, and A. Pawlina, "Attenuation and

scintillation statistics with Olympus and Italsat satellites in Italy," *Alta Frequenza*, vol. 6, no. 6, pp. 66–69, 1994.
[9] U. Merlo, E. Fionda, and J. Wang, "Ground level refractivity and scintillation in space-earth links," *Appl. Opt.*, vol. 27, pp. 2247–2252, 1987.
[10] Y. Karasawa, M. Yamada, and J. Allnutt, "A new prediction method for tropospheric scintillation on earth-space paths," *IEEE Trans. Antennas Propagat.*, vol. 36, pp. 1608–1614, Nov. 1988.
[11] "Effects of tropospheric refraction on radio-wave propagation," in Rep. CCIR Propagat. Nonionized Media, Int. Telecommun. Union (ITU), Rep. 718-3, Annex to vol. V, Geneva (CH), 1990, pp. 172–176.
[12] G. Ortgies, "Prediction of slant-path amplitude scintillation from meteorological parameters," in *Proc. Int. Symp. Radio Propagat.*, Beijing, China, 1993, pp. 218–221.
[13] E. Vilar and J. Haddon, "Measurement and modeling of scintillation intensity to estimate turbulence parameters in an earth-space path," *IEEE Trans. Antennas Propagat.*, vol. AP-32, pp. 340–346, Apr. 1984.
[14] F. S. Marzano and G. d'Auria, "Estimation of intermittent scintillation on microwave links from meteorological data," *Alta Frequenza*, vol. 6, no. 6, pp. 94–97, 1994.
[15] G. Schiavon, D. Solimini, and E. R. Westwater, "Performance analysis of a multifrequency radiometer for predicting atmospheric propagation parameters," *Radio Sci.*, vol. 10, pp. 631–650, 1993.
[16] E. R. Westwater, J. B. Snider, and M. J. Falls, "Ground-based radiometric observation of atmospheric emission and attenuation at 20.6, 31.65 and 90.0 GHz: A comparison of measurements and theory," *IEEE Trans. Antennas Propagat.*, vol. 38, pp. 1569–1580, 1990.
[17] P. Ciotti, P. Basili, G. d'Auria, F. S. Marzano, and N. Pierdicca, "Microwave radiometry of the atmosphere: An experiment from a sea-based tower during the ERS-1 calibration," *Int. J. Remote Sensing*, vol. 5, pp. 133–148, 1995.
[18] D. Vanhoenacker and A. Vander Vorst, "Experimental evidence of a correlation between scintillation and radiometry at centimeter and millimeter wavelengths," *IEEE Trans. Antennas Propagat.*, vol. AP-33, pp. 40–47, Jan. 1985.
[19] V. I. Tatarskii, *Wave Propagation in a Turbulent Medium.* New York: McGraw-Hill, 1961.
[20] A. Ishimaru, *Wave Propagation and Scattering in Random Media.* New York: Academic, 1978.
[21] V. I. Tatarskii and V. U. Zavorotni, "Wave propagation in random media with fluctuating turbulent parameters," *J. Opt. Soc. Amer.*, vol. 2, pt. A, pp. 2069–2076, 1985.
[22] G. d'Auria, F. S. Marzano, and U. Merlo, "Model of the refractive-index structure constant in intermittent clear-air turbulence," *Appl. Opt.*, vol. 32, pp. 2674–2680, 1993.
[23] T. E. Van Zandt, J. L. Green, K. S. Gage, and W. L. Clark, "Vertical profiles of refractivity turbulence structure constant: Comparison of observations by the sunset radar with a new theoretical model," *Radio Sci.*, vol. 13, pp. 819–829, 1978.
[24] G. d'Auria, F. S. Marzano, and U. Merlo, "Effects of intermittence on the refractive-index structure constant," in *Proc. ICO Meet. Atmosph., Vol., and Surface Scattering and Propagat.*, Firenze, Italy, 1991, pp. 87–91.
[25] T. J. Mousley and E. Vilar, "Experimental and theoretical statistics of microwave amplitude scintillations on satellite down-links," *IEEE Trans. Antennas Propagat.*, vol. AP-30, pp. 1099–1106, June 1982.
[26] F. Rucker and F. Dintelmann, "Effects of antenna size on OTS signal scintillations and their seasonal dependence," *Electron. Lett.*, vol. 19, pp. 1032–1034, 1983.
[27] E. Kessler and B. Neas, "On correlation, with applications to the radar and raingage measurements of rainfall," *Atmospher. Res.*, vol. 34, pp. 217–229, 1994.
[28] O. P. Banjo and E. Vilar, "The dependence of slant path amplitude scintillations on various meteorological parameters," in *Proc. 5th Int. Conf. Antennas Propagat. (ICAP'87)*, York, U.K., Apr. 1987, pp. 277–280.
[29] H. Liebe, "An atmospheric millimeter-wave propagation model," *Int. J. Infrared Millimeter Wave*, vol. 10, pp. 367–378, 1989.

Frank S. Marzano received the Laurea degree (*cum laude*) in electrical engineering and the Ph.D. degree in applied electromagnetics, both from the University "La Sapienza," Rome, Italy, in 1989 and 1993, respectively.

In 1993, he joined the Italian Space Agency and the Department of Electronic Engineering, University "La Sapienza," Rome, Italy, as a Postdoctorate Researcher. In 1997, he joined the Department of Electrical Engineering, University of L'Aquila, Italy where he is currently an Assistant Professor. Since 1990, he has been participating in many international projects on remote sensing and telecommunications (MAC-Europe in 1991, GPCP-AIP-2 in 1992, NASA PIP-2 in 1994, GPCP-AIP-3 in 1995, COST-255 in 1996, and COST-712 in 1997). His research mainly concerns passive and active remote sensing of the atmosphere from airborne and spaceborne platforms, with a special focus on precipitation and inversion method development, radiative transfer modeling of scattering media, and analysis of tropospheric scintillation along satellite microwave links.

Dr. Marzano received the Young Scientist Award of the XXIV General Assembly of the International Union of Radio Science (URSI) in 1993.

Giovanni d'Auria was born in Rome, Italy, on June 23, 1931. He received the degree in electrical engineering and the Libera Docenza degree, both from the University "La Sapienza," Rome, Italy, in 1956 and 1964, respectively.

He served in the Italian Air Force, working in ITAV Laboratories. He was with Fondazione Ugo Bordoni as Researcher in the Antennas and Propagation Laboratory. He joined the Department of Electronics, University of Rome as an Assistant Professor, in 1962, teaching applied electronics. In 1976, he was appointed Professor in the Chair of Antennas and Propagation and has been teaching this subject ever since. His current research concerns electromagnetic propagation in a turbulent atmosphere, microwave remote sensing of the atmosphere and earth's surface, microwave radiometry of the atmosphere, and particularly of cloud systems.

Dr. d'Auria has been an official member of Comm. F of the Italian Committee of URSI, since 1996.